Published in final edited form as:
Magn Reson Med. 2006 January ; 55(1): 30–40.

Highly Constrained Backprojection for Time-Resolved MRI

C. A. Mistretta[1,2,3,*], **O. Wieben**[2], **J. Velikina**[1], **W. Block**[1,3], **J. Perry**[1], **Y. Wu**[1], **K. Johnson**[3], and **Y. Wu**[1]

1*Department of Medical Physics, The University of Wisconsin-Madison, Madison, WI, USA.*

2*Department of Radiology, The University of Wisconsin-Madison, Madison, WI, USA.*

3*Department of Biomedical Engineering, The University of Wisconsin-Madison, Madison, WI, USA.*

Abstract

Recent work in k-t BLAST and undersampled projection angiography has emphasized the value of using training data sets obtained during the acquisition of a series of images. These techniques have used iterative algorithms guided by the training set information to reconstruct time frames sampled at well below the Nyquist limit. We present here a simple non-iterative unfiltered backprojection algorithm that incorporates the idea of a composite image consisting of portions or all of the acquired data to constrain the backprojection process. This significantly reduces streak artifacts and increases the overall SNR, permitting decreased numbers of projections to be used when acquiring each image in the image time series. For undersampled 2D projection imaging applications, such as cine phase contrast (PC) angiography, our results suggest that the angular undersampling factor, relative to Nyquist requirements, can be increased from the present factor of 4 to about 100 while increasing SNR per individual time frame. Results are presented for a contrast-enhanced PR HYPR TRICKS acquisition in a volunteer using an angular undersampling factor of 75 and a TRICKS temporal undersampling factor of 3 for an overall undersampling factor of 225.

Keywords

time resolved MRI; constrained backprojection; undersampled data; ultra-fast imaging; acceleration factors

There are many applications for which it is desirable to have high spatial and high temporal resolution. K-space sampling that obeys the Nyquist theorem usually precludes simultaneous achievement of these aims in MR imaging. Among other approaches, radial acquisitions have been proposed for accelerated sampling schemes. Peters (1) and Vigen (2) reported on the use of 3D MR angiography acquisitions in which 2 dimensions were encoded using undersampled projection reconstruction and the third was encoded using phase encoding. In these applications, the projections are rotated around a single axis and, even if the planes containing the projections are completely sampled in the Fourier encoded direction, the undersampling factor, relative to that required by the Nyquist theorem, is limited to about 6 due to the streaks in the axial reformatted images.

When radial sampling is extended by distributing the projections in all directions in 3D as in VIPR (3), significantly higher acceleration factors relative to fully sampled acquisition can be achieved. We recently reported on a relatively artifact free PC VIPR (phase contrast Vastly undersampled Isotropic PRojection imaging) acquisition in which an acceleration factor of 61 relative to conventional Cartesian 3D PC was achieved (4). This acceleration factor was defined

*Correspondence to: Charles A. Mistretta, Clinical Science Center, J5/M172, 600 Highland Avenue, Madison, Wisconsin, 53792, USA. E-mail: camistre@wisc.edu

as the ratio of an imaging speed index for PC VIPR and Cartesian 3D PC acquisitions. This index was determined as the volume covered divided by the product of scan duration times voxel size.

Despite such large increases in acquisition speed, some applications would benefit from further accelerations. For example, in recent cine PC VIPR measurements with 3D flow encoding for pressure mapping in 1–2 mm thick vessels using an acquisition matrix of 256 × 256 × 256 voxels and 10 cardiac phases in a 10-minute scan time, we underestimated the velocities in peak-systole by about 13% (5). In this work, 2000 VIPR projections were collected for each of the cardiac phases. This represents an undersampling factor of 50 relative to the Nyquist requirement of approximately 100,000 projections for a 256^3 image matrix. It would be desirable to further increase the number of available cardiac phases and also to further reduce the scan time.

In the case of time-resolved contrast-enhanced VIPR studies, the streak artifacts have been reduced using a spatial frequency dependent (Tornado) filter (3) in which the temporal window is increased as the radial distance from the center of *k*-space increases. This reduces streak artifacts but causes vessel edges to have a reduced temporal bandwidth and to appear too early in the reconstructed time sequence. It would be desirable to reduce this effect.

Recently, the k-t BLAST technique has been proposed (6,7). With this technique, it is recognized that an acquired time series contains large amounts of correlated information in the *k*-space data associated with a set of time frames. In k-t BLAST, which has also been applied to radial acquisitions (7), a low spatial frequency training data set is acquired to remove the aliasing that occurs when undersampling is performed in the spatial and temporal domains. Using an iterative reconstruction, significant reductions in the required data can be achieved. Huang, Gurr, and Wright (8) have reported on an MR angiographic technique that also incorporates the idea of using a training set to guide the reconstruction of 3D images using pairs of orthogonal 2D projection images, similar to modern X-ray DSA acquisitions. In this method an iterative reconstruction is guided using correlation analysis of data from a training set that is comprised of all acquired orthogonal 2D projection images. This method also has the potential to significantly improve acquisition speed for time-resolved series.

Here we present an approximate reconstruction method based on a non-iterative, unfiltered, constrained back-projection reconstruction to improve the achievable temporal resolution in radial MR imaging. With this approach, the reconstruction of individual time frames is achieved by limiting the back-projected information to voxels defined to be vessels in the composite image generated from all acquired projections. It uses a back-projection weighting defined by the intensities in the composite image. The method provides an additional acceleration factor beyond that provided by undersampled radial acquisition and is applicable to time resolved acquisitions using arbitrary *k*-space trajectories. The method is best suited for situations in which temporal signal changes are similar at all spatial positions but can be adapted to accommodate situations such as delayed filling of peripheral arteries. The objects in the imaging volume should also not change positions over the time frames.

METHODS

Theory

The basic acquisition and reconstruction technique, which we will refer to as HYPR for **H**igh**Y** constrained back-PRojection, is illustrated schematically in Fig. 1. The data are ideally acquired in the form of time frames containing interleaved and equally spaced *k*-space projections. All of the acquired data are combined and used to reconstruct a composite image, either by filtered backprojection or by regridding and a subsequent inverse Fourier transform.

A HYPR time frame is reconstructed by multiplying the composite image by backprojections generated by calculating the Fourier transform (image space profile) of each time frame radial *k*-space projection and normalizing them by the corresponding image space profile from the composite image. The contributions from all projections in the time frame are summed.

The data reconstruction method is illustrated in Fig. 2 for the case of a single VIPR projection characterized by the spherical coordinates θ, ϕ, and *r*. At each radial location, *r*, the value of the image space profile obtained by Fourier transformation of a *k*-space projection within a time frame is spread into the Radon plane perpendicular to the orientation of the radial *k*-space line. Instead of a filtered backprojection process in which projection values are filtered and uniformly distributed into the Radon plane, the projection value is distributed in the Radon plane using information from the composite image. The profile value is weighted at points x, y, and z in the plane based on the image intensity at the corresponding points in the composite image. This is achieved through simple multiplication of the normalized profile value by the composite image. The product is normalized by the corresponding profile value of the composite image. The formula for the reconstruction is

$$\text{HYPR image}\,(x,y,z) = \left(1/N_{pr}\right)^{*} \quad C(x,y,z)^{*} \; \Sigma\left[P(r,\theta,\varphi)/P_c(r,\theta,\varphi)\right] \qquad [1]$$

where the sum is calculated over all projections in the current time frame for which the corresponding (r,θ,ϕ) Radon plane contains the point (x,y,z). N_{pr} is the number of projections in the time frame. P(r,θ,ϕ) is the profile value for this plane, P_C(r,θ,ϕ) is the corresponding value calculated from the time-averaged composite image, and C(x,y,z) is the composite image itself.

An example containing 2 vessels only is shown in Fig. 2 to visualize this method. Each, for simplicity, passes through 1 voxel in the Radon plane at location *r*. The signal in the projection P(r,θ,ϕ) obtained at r following Fourier transformation of the acquired VIPR *k*-space projection is shared with all voxels within the associated Radon planes. This is accomplished using weighting factors calculated from the time-averaged composite image that has signal values of w1 and w2 for arteries 1 and 2. In the simple case illustrated in Fig. 2, the signal contributions for a single projection in the Radon plane passing through r for vessels 1 and 2 are given by Eq. [1] as

$$S_1 = w_1{}^{*}P/(w_1 + w_2) \quad S_2 = w_2{}^{*}P/(w_1 + w_2) \qquad [2]$$

For a 2D projection distribution, the information detected at each point in the image space profile would be back-projected to those vessel voxels lying on a single straight line perpendicular to the projection.

The HYPR reconstruction dramatically reduces streak artifacts in the space between vessels for a time-resolved imaging sequence. In the limiting case in which all of the vessels have the same temporal waveform, this process appropriately distributes the projected intensity into the correct locations and eliminates vessel-to-vessel streak artifacts. In this specific case, a complete and error-free reconstruction can be achieved with a single projection per time frame. In practical applications, where there may be significant differences in the temporal behavior at different points in space, results are improved as greater numbers of projections are acquired per time frame. This will be illustrated in the simulations.

The spatial resolution of the HYPR image is determined by the spatial resolution of the composite image. Therefore, without application of reregistration techniques based on the projection information (9), the technique is limited to situations in which vessel positions remain stationary during the acquisition either because they are not moving or because ECG gating is employed.

The HYPR reconstruction can be applied to acquisitions using arbitrary *k*-space trajectories by regridding the acquired *k*-space data into projections proceeding as above. However, direct acquisition of the projections is likely to be most effective.

Noise Considerations

The individual time frame projection, the projection through the composite image, and the composite image itself can contribute to the stochastic noise in the image calculated using Eq. [1]. In the Appendix it is demonstrated that the SNR in the reconstruction of each time frame is dominated by the composite image. In this article, SNR is calculated as the ratio of vessel signal to the noise SD within the vessel. CNR is calculated as the difference between the vessel and background signals divided by the SD of the background noise. The overall SNR and CNR are limited by a combination of the stochastic noise and the noise due to streak artifacts. It is shown in the Appendix that the stochastic component of the SNR in the HYPR image is given by:

$$SNR_{HYPR} = SNR_{composite} / \left[1 + N_f / N_v^2 + N_{pix} / \left(N_p N_v^2 \right) \right]^{1/2} \quad [3]$$

where $SNR_{composite}$ is the SNR in the composite image, N_f is the number of frames in the time series, N_v is the number of vascular pixels in the projection, N_{pix} is the number of pixels in the projection (e.g., 256 for 2D or 256 × 256 for 3D), and N_p is the number of projections per time frame. For the simulations presented in this article, N_v is on the order of 10 and the SNR is dominated by $SNR_{composite}$. For the case of a single vascular pixel, the second and third terms in the denominator of Eq. [3] dominate. These correspond to the noise in the time frame projection and the composite image projection, respectively.

Some of the following simulations will further explore the SNR and CNR properties of the HYPR method.

Simulations

Although the HYPR technique may be applied in 2DPR or in 3D VIPR we have, for simplicity, simulated the HYPR concept in 2 dimensions using MATLAB (The Mathworks Inc. Natick, MA, USA). Three simulations have been implemented. The first image set was generated from an ECG gated PC VIPR data set with regional variations in the temporal behavior of the signal. This simulation was intended to investigate the accuracy of the temporal waveforms derived from the HYPR algorithm in the presence of spatial variations of the temporal waveform. The second simulation was designed to investigate the SNR characteristics of the HYPR technique. In particular, an estimate of the achievable increase in scan speed through reduction in the number of projections per frame relative to conventional undersampled acquisition was the goal of this simulation. The third simulation investigates the behavior of HYPR for contrast-enhanced MRA with delayed vessel filling in one region of the field of view.

Simulation One—In the first simulation, designed to investigate non-stochastic streak artifacts, a maximum-intensity projection (MIP) time frame from a time resolved PC VIPR series was regarded as a relatively artifact free image and used to artificially generate 16 time frames. No additional noise was added. The original time frame was weighted differently on the right and left sides of the image, with the left side being modulated with a peak-to-peak sinusoidal signal variation representing 40% of the mean signal while the right side was kept constant. Images from 2 time frames having minimum and maximum signal values on the left side of the field of view are shown in Fig. 3. The sinusoidal modulation was varied to produce one half, 2, or 4 cycles of the intensity variation per cardiac cycle on the left side while the right side remained unchanged.

The original image used to generate the time series was well sampled in projection angle. Simulations were performed assuming just 4, 6, 8, or 10 projections per time frame. A composite image was formed by using the assumed number of projections in each of these time frames and summing over all time frames.

For each time frame the HYPR algorithm was applied at each projection angle and the results were summed to form the HYPR image time frame. Conventional filtered back-projection images, referred to here as FBP images, using the same number of projections per time frame as the HYPR frame used, were reconstructed for comparison with the HYPR images.

ROIs comprising 32 pixels were drawn in the middle cerebral arteries on the right (unmodulated) side and the left (modulated) side and were used to generate temporal waveforms for the input image series and the HYPR and FBP image series. The accuracy of the temporal waveforms and the image quality of all 3 series were compared.

Simulation Two—The second simulation was designed to demonstrate the relative roles of stochastic and non-stochastic noise in the phase contrast MRA time series. In this simulation HYPR images were generated for several different combinations of projections per image and numbers of cardiac phases. The vessel image quality was compared with that of a conventional undersampled FBP image formed from 40 projections.

Gaussian noise equal to 3% of the peak vascular signal was added to each of the 16 input images. A fully sampled image with 400 projections was generated from the first of these images in the time series. The CNR values for the various cases illustrated in the Results section were expressed as ratios relative to the values in the fully sampled image.

Simulation Three—The third simulation represents the use of HYPR for contrast enhanced MRA. A series of 11 time frames from a PR TRICKS acquisition (2) were represented by their MIP images and used to test the properties of the HYPR algorithm. PR TRICKS is a hybrid 3D technique employing Cartesian temporal undersampling in 1 dimension and undersampled projections in 2 dimensions. In this series, there was delayed filling in one of the legs. In such cases the use of a composite image comprised of all frames can potentially alter the observed time course because all vessels will be filled in the composite image. These composite image vessels can deposit signal in voxels in early frames before contrast material has actually arrived. To avoid such errors in the HYPR images, a progressive series of composite images was used instead. For the first time frame, only the first 2 images in the series were used to form the composite image for the HYPR reconstruction. For each additional time frame, an additional image from the series was added to the composite image. This is illustrated in Fig. 4. For example, using this scheme, for the fifth time frame, 6 time frames of data would be included in the composite C5. The HYPR time series and the FBP time series were reconstructed using 30 projection angles.

PR HYPR TRICKS Volunteer Study—PR TRICKS data were acquired using a 17 cc injection of Omniscan at 2cc/s. Ten projections per time frame were used. The current implementation of the sequence limits the number of projection interleaves to 20, resulting in 200 independent projections being available for the composite image, thus reducing the potential SNR gain. For the in-plane matrix of 512 × 512, the 10 projections represented an angular undersampling factor of 75. The TRICKS partitioning on the slice encoding direction used 3 *k*-space regions, producing a temporal undersampling of 3, resulting in a combined undersampling in k and t of 225. FBP and HYPR signal curves from 2 regions of interest were compared. HYPR was applied on a slice by slice basis.

RESULTS

Figure 5 shows the results of reconstructing the first time frame from the original series of phase contrast MIP images before adding the additional left/right modulation. FBP and HYPR reconstructions using 4, 6, 8, and 10 projections are shown. FBP images reconstructed with so few projections do not allow for the recognition of the imaging scene while the HYPR images demonstrate diagnostic image quality.

One of the properties of the HYPR algorithm is its ability to reduce intravascular streak artifacts. This is due to the knowledge of where to deposit the backprojected signal based on the composite image information. In Fig. 6 the 10-projection HYPR image of Fig. 5 is compared with an image formed by a simpler algorithm in which a 10-projection FBP image is multiplied by the composite image. Once the intravascular streak artifacts have been formed by the FBP process, they cannot be removed by multiplication with the composite image.

Simulation One—Waveform Behavior

Figure 7 shows the waveforms for the left (modulated) side of the image. The measured waveforms for the HYPR reconstruction were exact for the special case in which one horizontal projection (summing vertical data) was used for reconstruction (not shown). This is due to the fact that there was no mixing of temporal behavior from the left side of the image to the right side. When a vertical and a horizontal projection are used, there is mixing and the HYPR waveform was significantly different from that of the programmed temporal behavior.

However, the HYPR waveform was in fairly good agreement with the programmed waveform when 4 or more projections were used from each time frame. The maximum and the mean errors for the 10-projection case were 9% and 3.5%, respectively. Although the FBP image quality was quite poor due to severe streaking artifacts, the FBP waveform was surprisingly good for 10 or more projections for this particular vessel configuration and temporal waveform distribution. These results were very similar for the one half, 2, and 4-cycle modulations.

Figure 8 shows the results for the right, unmodulated side. There is some mixing of temporal behavior from the left to the right side, resulting in non-constant waveforms on the left side. For the 10-projection case, the maximum error is 12% and the average error is 5%. This result is fairly independent of the number of projections used from each time frame

Simulation Two—SNR Behavior

Figure 9 compares HYPR images generated with several combinations of projections per time frame and total numbers of time frames. The SNR values involving the SD of the pixel values were somewhat difficult to compare with the predicted values using the formulas in the Appendix. This was due to contributions to the SD from anatomic variations in the vessel signal. CNR values were quite reliable and are relative to a fully sampled image with 400 projections. The CNR value in the standard 40-projection FBP image is decreased by more than the factor of the square root of 10 from reducing the scan time by 10. This is due to the presence of non-stochastic noise originating from undersampling artifacts. When the HYPR technique is applied with 40 projections in each of the time frames of a 30 frame temporal acquisition, the CNR is increased by a factor of 6 relative to corresponding 40-projection FBP time frames in a series requiring the same imaging time. For a 20-frame acquisition, the image quality of a 4-projection per time frame HYPR image is better than that of the 40-projection FBP image and increases further for a 30-frame acquisition where, in addition to a factor of 10 increase in imaging speed per time frame, the CNR is more than doubled.

Simulation Three—Contrast Enhanced Angiography

Figure 10a (top row) shows 8 MIP image time frames from a PR TRICKS acquisition. These images were acquired with 150 projections per frame and are relatively artifact free. The series shows delayed filling on the left side of the field of view (right leg).

Figure 10a (middle row) shows the image series acquired when these time frames are subjected to reprojection and filtered backprojection using only 30 projection angles. Streak artifacts are severe and the images are of non-diagnostic quality. Figure 10a (bottom row) shows the time series reconstructed with the HYPR method. Streaks are significantly reduced compared to the FBP images. The image quality improves with the frame number due to the increasing numbers of projections in the sequence of composite images used. Figure 10b shows the signal curves for FBP, HYPR, and the Actual waveform used as input to the simulations. For the first 2 frames, the FBP and HYPR overestimate the signal due to the presence of streak artifacts. HYPR streak artifacts are reduced as more projections are added to the composite mask.

Figure 11 displays the results of the PR HYPR TRICKS volunteer study. Figure 11a shows every fifth 940ms FBP time frame. Image quality is unacceptable due to streak artifacts and low SNR due to the use of just 10 projections per time frame. Figure 11b shows the HYPR results, which demonstrate greatly improved SNR and streak reduction.

DISCUSSION

The simulations performed here represent the expected performance of HYPR in acquisitions in which the projection angles are rotated around a fixed axis as in PR TRICKS (2) and PIPR (**P**hase **I**maging with **PR**ojections) (10). In such applications, standard reconstruction of an undersampled projection set permits undersampling factors of about 6 before artifacts become objectionable when axial reformatted images oriented perpendicular to the projection rotation axis are viewed. For phase contrast applications using this acquisition geometry, HYPR provides an additional acceleration factor of about 25 depending on the number of cardiac phases in the acquired data. For contrast enhanced angiography in anatomic regions where late filling is a potential problem, such as in Simulation 3, Fig. 10 shows that the use of a progressive series of composite images leads to a variable increase in the HYPR image quality from the first frame to the eighth frame.

When undersampled projection imaging was extended from a 2-dimensional distribution to the 3-dimensional VIPR trajectory, which varies both the polar and azimuthal orientations of the projections, undersampling factors were increased by another factor of 10, resulting in undersampling factors of about 50 (5). This is because the artifactual spreading of signal from one source to another falls off according to $1/r^2$ as opposed to 1/r as in the purely azimuthal case. This $1/r^2$ behavior associated with the VIPR trajectory and the use of greater numbers of projections in the VIPR case will also likely reduce the potential distortion of the measured temporal waveforms when applying the HYPR technique, thereby reducing the number of required projections by greater factors and reducing the need for a progressive mask series. This $1/r^2$ reduction of artifact signal level would very likely reduce the contamination of the waveforms observed in Simulation 1. Additional studies are needed to test this hypothesis. In general, contamination will also be reduced as the density of signal voxels is reduced. Therefore, HYPR is best suited for data sets such as those in angiography where the occupied voxel fraction is on the order of 0.2%. However, other data sets, such as activation signal distribution in fmri, should also be considered for potential application.

The potential implications of the HYPR technique can be appreciated by considering how the acquisition parameters might be changed for our recently reported measurements of pressure drops in small vessels (5). In that work we use a 256 × 256 × 256 acquisition matrix and obtain

3-component velocity information in 10 cardiac phases in about 10 minutes. The angular undersampling factor relative to the fully sampled 100,000 projections required by the Nyquist theorem is about 50, resulting in about 2000 projections per cardiac phase. If 30 HYPR time frames were used and, as our calculations in the Appendix suggest, gains similar to those shown in the 2D simulations presented here also hold for VIPR, the number of projections per phase could be further reduced by a factor of 10 without additional undersampling artifacts. Although we have only presented 2D simulations here, this would result in an overall undersampling factor of 500 in the 3D case and would permit, for example, an increase in the number of cardiac phases from 10 to 30 and a reduction of the scan time from 10 minutes to about 3 minutes simultaneously. Current ungated PC VIPR results (4) suggest that the SNR in a 3-minute composite image will support this reduction in scan time. Our calculations (Appendix) also predict a 70% increase in SNR in this case. The scan time for a 3D Cartesian phase contrast scan providing 256 × 256 × 256 with 3 components of velocity and 30 time frames, assuming a TR of 10 ms and a 4 point acquisition (1 reference + 3 velocity encodings), would be 21.3 h.

Figure 12 summarizes the time frame acceleration factors associated with several undersampled projection acquisition schemes in MR angiography. The undersampling strategies employed are indicated by *k* for purely *k*-space undersampling, *t* for purely temporal undersampling, *k*-*t* for a combination of *k*-space and temporal undersampling, and *k*-*t** when the *k*-*t* strategy also employs the concept of exploiting the composite image to guide the reconstruction. The acceleration factors reflect the time-savings for the acquisition of individual frames. For the HYPR technique, it is necessary that there be on the order of 10–30 time frames and an adequate number of summed projections so that a sufficient SNR and streak reduction can be achieved in the composite image. Therefore, accelerations in scan time must be calculated with this constraint in mind. The hybrid undersampled PR technique (1), which undersamples the azimuthal angle relative to a single axis, typically permits time frame acceleration factors of about 6, based purely on undersampling of *k*-space in the azimuthal direction. The PR TRICKS technique (2) combines undersampling in *k*-space and time and produces accelerations of about 18. PC VIPR has produced acceleration factors of 50, due entirely to the combination of polar and azimuthal *k*-space undersampling. The combination of HYPR with undersampled Hybrid PR produces acceleration factors on the order of 100, as indicated by comparison of the 400-projection and 4-projection images in Fig. 8. This is a factor of 25 beyond what is achievable using undersampled Hybrid PR alone. The combination of TRICKS with undersampled Hybrid PR resulted in an undersampling factor of 225 (Fig. 11). This is due to the additional benefits of combining *k*-space and temporal undersampling along with constrained reconstruction (6-8). The composite mask supports a much higher SNR in the individual time frames compared with the usual square root of time SNR dependence one would experience for the acquisition of a single frame.

The issue of SNR is an important one for all acceleration techniques, including VIPR and parallel imaging. With an additional order of magnitude increase in acquisition speed from VIPR to HYPR VIPR, acceleration factors will be available that will be capable of providing frame rates and voxel size reductions well beyond those that can be supported by the available SNR in some applications. However, as additional SNR is provided by improved coils, higher field strengths, improved contrast material, or perhaps hyperpolarization methods, these highly undersampled techniques will be increasingly useful.

The HYPR technique exploits the important concept of using data obtained throughout the acquisition of the time series to assist in the reconstruction of the individual time frames. This concept is clearly stated in the k-t BLAST literature (6,7) and in the recent work of Huang, Gurr, and Wright (8). HYPR reconstruction is a simple non-iterative method, applicable to any time-resolved set of *k*-space trajectories, and performs constrained backprojection based on

vessel positions defined in the composite image. For the limiting case in which the temporal variation of signals in all parts of the imaging volume remain fixed from frame to frame, the image volume and waveform can be determined using a single projection per frame. This is reminiscent of the situation discussed by Hennig in his plenary lecture at the ISMRM meeting (11), where a time series was generated using a single central *k*-space point to modulate the intensity of a known image with a spatially uniform time dependence. For realistic imaging situations, the number of required projections will increase as the temporal behavior becomes more heterogeneous.

For situations where significant spatial variations are present in the temporal behavior, the progressive composite image approach allows for the extension of the technique but at the cost of reduced gains in the SNR, which will vary within the time series. The progressive mask concept can be extended to allow for imaging in the venous phase if desired. In this case the earlier time frames would be excluded from the composite images used for the reconstruction of venous phases.

The HYPR technique was applied to phase contrast complex difference speed images in the simulations presented here. For situations in which it is desired to retain the sign of the velocity, the complex difference image can be used to form the composite image. The time frame projections would be taken through the time frame phase images and the normalizing projections would be taken through the complex difference composite image.

HYPR time frames can have much higher SNR compared with conventional filtered backprojection images produced with the same number of projections. Since the projection information for the time frame is an integral of signal and noise over a line (2D) or a plane (3D), SNR can be greater than what would be calculated based on consideration of individual time frame image elements. Because HYPR removes streak signal from the space between vessels, the streaks (2D) or background haze (3D) from angular undersampling will be reduced. The spreading of signal from one vessel to another vessel will also be reduced by the first order approximation of spatially uniform temporal behavior. As emphasized above, all of these applications must be evaluated in the context of particular clinical applications and available SNR.

In the simulations presented here, it has been assumed that the vessel distribution is spatially stationary. For applications in which motion can occur in the time series of images, it might be possible to extend the HYPR technique by using the information from the acquired projections to correct for rotation and translation in the imaging scene (9) so that the information in the individual time frames and the training set can be aligned properly.

CONCLUSIONS

The HYPR method can be used to increase the SNR of time frames or to reduce scan time for fixed time frame SNR and artifact level in imaging scenes with high contrast and sparse signal distribution, such as CE-MRA and PC imaging. For 2D applications, our simulations indicate that angular undersampling factors of 100 may be possible within the limits of available SNR. Additional simulations and in vivo experiments are required to verify that similar behavior will be seen for 3D VIPR acquisitions, where undersampling factors on the order of several hundred may be possible. The degree of temporal waveform distortion is likely to be significantly less for VIPR acquisitions as compared with the 2D simulations. The HYPR technique can be applied to acquisitions using arbitrary *k*-space trajectories for which projections can be synthesized from the acquired data but is ideally suited to radial acquisitions where all *k*-space data are grouped into interleaved projections.

ACKNOWLEDGMENTS

The authors gratefully acknowledge helpful discussions with Sean Fain.

Grant Sponsor: NIH; Grant Numbers: 1RO1HL/RR66488–01A1 and 1R01HL72260–01. Grant Sponsor: GE Healthcare.

APPENDIX A: SIGNAL TO NOISE RATIO CONSIDERATIONS

In this Appendix we calculate the stochastic component of the noise in the HYPR images, which is usually dominated by the noise in the composite image.

The HYPR time frame image component associated with a single projection is calculated as

$$H = \left(1/N_p\right)^* \sum_{0}^{Np-1} \left[C^* P_t / P_c\right] \quad [A1]$$

where P_t is a projection acquired during the time frame and P_c is the corresponding projection through the composite image C, and the sum is calculated over all projections in the time frame. The total differential of H is given by:

$$\Delta H = \left(1/N_p\right)^* \left[\sum_{0}^{Np-1} (\Delta C)^* (P_t/P_c) \quad + \Sigma(\Delta P_t)^* (C/P_c) + \quad \Sigma(\Delta P_c)^* \left(C^* P_t / P_c^2\right)\right] \quad [A2]$$

The signal in each time frame projection is given by $P_t \approx (N_v * C) \approx P_c$, where N_v is the number of vascular pixels included in the projection. The mean vascular signal is assumed to be C. The noise in the composite image is the same for each projection and will add coherently in each voxel. The other noise components will add as uncorrelated noise samples. Correlation between the noise in PC and C will be ignored. With these assumptions we get:

$$(\Delta H)^2 = \left(1/N_p\right)^{2*} \left[\left(N_p \Delta C\right)^2 + \quad N_p (\Delta P_t)^{2*} (C/P_c)^2 + N_p (\Delta P_c)^{2*} \left(C^* P / P_c^2\right)^2\right] \quad [A3]$$

ΔP_t is an average over the number of readout points in the projection, usually 256, and is given by $\Delta P_t = \sigma / N_r^{1/2}$ where σ is the noise per readout sample. The noise in the composite image is an average over the number of projections per time frame N_p, the number of time frames N_f, and the number of readout points N_r, and is given by $\Delta C = \sigma / (N_r N_p N_f)^{1/2}$. The error in the projection through the composite image is increased by the square root of the number of pixels N_{pix} in the projection, i.e., $\Delta P_c = \sigma^* (N_{pix})^{1/2} / (N_r N_p N_f)^{1/2}$.

Substituting these values we obtain:

$$(\Delta H)^2 = \left(\sigma^2 / N_r N_p N_f\right)^* \left[1 + N_f / N_v^2 + N_{pix} / \left(N_p N_v^2\right)\right] \quad [A4]$$

The SNR for the HYPR time frame including all projections is then given by:

$$SNR_{HYPR} = C\left(N_r N_p N_f\right)^{1/2} / \left\{\sigma^* \left[1 + N_f / N_v^2 + N_{pix} / \left(N_p N_v^2\right)\right]^{1/2}\right\} \quad [A5]$$

$$= SNR_{composite} / \left[1 + N_f / N_v^2 + N_{pix} / \left(N_p N_v^2\right)\right]^{1/2} \quad [A6]$$

The first term in this sum is due to the error in the composite image and usually determines the SNR. Using the fact that the SNR in a filtered backprojection image is $C (N_r N_p)^{1/2} / \sigma$, we can calculate the ratio of SNR for HYPR and FBP images for various cases.

For the case of a 40-projection FBP image and a 30 frame series of 40-projection HYPR images, we predict that $SNR_{HYPR} = 5.2\ SNR_{FBP}$. This is approximately the square root of the number of frames, which is a reflection of the fact that SNR is dominated by the composite image, which increases SNR at that rate. In Fig. 8 the simulations show that the SNR for a 4-projection time frame from a 30 frame HYPR series has a factor of 2 increase in CNR relative to the 40 projection FBP image. Our equations predict a ratio of 1.7 for this case based on purely stochastic noise considerations. We presume the additional increase in CNR is due to reduction of streak artifacts due to the greater number of projections in the composite image.

In the above calculation we have assumed that $N_v = N_{pix}*f$ where f is a vascular sparsity factor representing the fraction of voxels that are occupied by vessels. In the 2D case using the VIPR MIP images for the simulation, this value was 0.1. When MIP images are not used, we have measured a sparsity factor of about 0.002. For this data set there is a tradeoff between SNR and the accuracy of the measured temporal waveforms depending on whether the HYPR algorithm is applied to the MIP images or individual slices, in which case the 0.002 factor would apply. For the 3D VIPR case, the 0.002 factor must be used since the HYPR algorithm must be applied in each Radon plane. In this case, waveform contamination should be significantly reduced relative to the 2D MIP case.

For the 3D case, the equations predict that if we increase our undersampling factor from the present PC VIPR value of 50 to a value of 500 by decreasing the number of projections from 2000 to 200 in a 30 frame sequence, the SNR of the 50 projection HYPR frames will be 1.7 times that of our current 2000 projection images. This is in spite of the additional factor of 10 increase in speed.

For applications such as phase contrast angiography where there is no background signal, CNR predictions are identical to SNR predictions. CNR predictions have been compared with the simulation due to the greater accuracy of determining a stochastic noise estimate free of intravascular velocity variations that would contribute to the estimated noise.

REFERENCES

1. Peters DC, Grist TM, Korosec FR, Holden JE, Block WF, Wedding KL, Carroll TJ, Mistretta CA. Undersampled projection reconstruction applied to MR angiography. Magn Reson Med 2000;43:91–101. [PubMed: 10642735]
2. Vigen KK, Peters DC, Grist TM, Block WF, Mistretta CA. Undersampled projection-reconstruction imaging for time-resolved contrast-enhanced imaging. Magn Reson Med 2000;43:170–176. [PubMed: 10680679]
3. Barger AV, Block WF, Toropov Y, Grist TM, Mistretta CA. Time-resolved contrast-enhanced imaging with isotropic resolution and broad coverage using an undersampled 3D projection trajectory. Magn Reson Med 2002;48:297–305. [PubMed: 12210938]
4. Gu T, Block WF, Korosec FR, Fain SB, Suleiman SA, Zhou Y, Grist TM, Mistretta CA. PC VIPR: a high resolution and high speed phase contrast method using 3D vastly undersampled isotropic projection imaging. American Journal of Neuroradiology 2005;26:743–749. [PubMed: 15814915]
5. Johnson, K.; Gu, T.; Mistretta, CA. 4D pressure mapping with time-resolved PC VIPR. ISMRM; Miami, Florida: 2005. Abstract 598
6. Tsao J, Boesinger P, Pruessman KP. k-t BLAST and k-t Sense: dynamic MRI with high frame rate exploiting spatiotemporal correlations. Magn Reson Med 2003;50:1031–1043. [PubMed: 14587014]
7. Hansen, MS.; Tsao, J.; Kozerke, S.; Eggers, H. k-t BLAST reconstruction from arbitrary k-t sampling: application to dynamic radial imaging; Proceedings of the 13th Annual Meeting of ISMRM; Miami Beach, Florida, USA. 2005. Abstract 684
8. Huang, Y.; Gurr, D.; Wright, G. Time-resolved 3D MR angiography by interleaved biplane projections; Proceedings of the 13th Annual Meeting of ISMRM; Miami Beach, Florida, USA. 2005. Abstract 1707

9. Wieben, O. Novel acquisition strategies for time-resolved 3D magnetic resonance angiography. The University of Wisconsin-Madison; 2002. Ph.D. thesis

10. Barger AV, Peters DC, Block WF, Vigen KK, Korosec FR, Grist TM, Mistretta CA. Phase contrast with interleaved undersampled projections. Magn Reson Med 2000;43:503–509. [PubMed: 10748424]

11. Hennig, J. Plenary Lecture, Fast imaging horizons in rapid MR imaging; Proceedings of the 13th Annual Meeting of ISMRM; Miami Beach, Florida, USA. 2005.

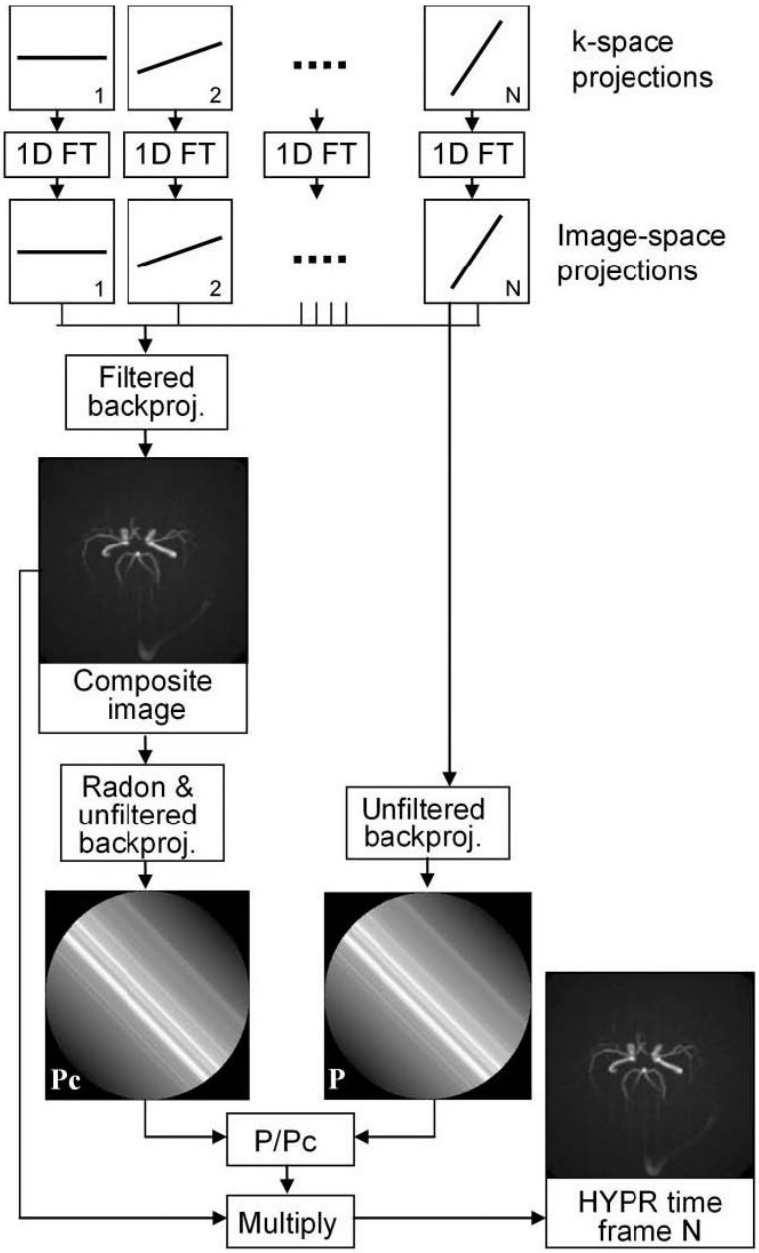

FIG. 1.

Schematic diagram of the HYPR reconstruction algorithm. For simplicity, the diagram shows a single projection for each time frame. A 1D Fourier Transform converts the radial *k*-space lines to projections in image space. A composite image is reconstructed from the projections in all time frames. For each individual HYPR time frame, the composite image is multiplied by the unfiltered backprojected profile P specific to the time frame normalized by the corresponding unfiltered backprojected profile P_c calculated from the composite image.

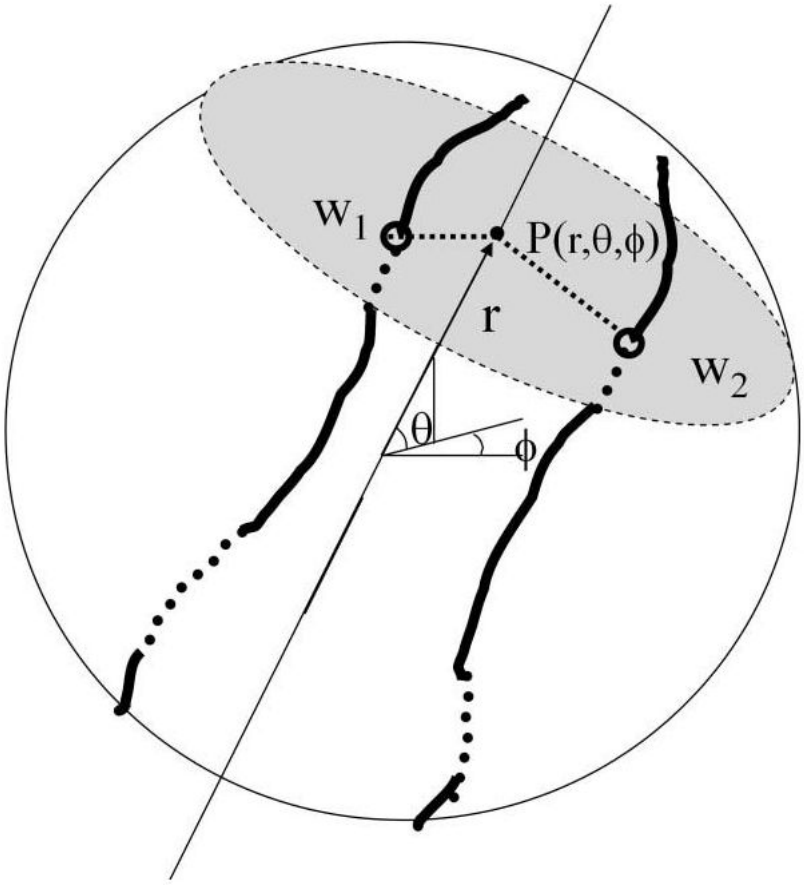

FIG. 2.

Illustration of the HYPR algorithm for the case of 3D VIPR. Each projection profile value is distributed in the Radon plane perpendicular to the profile in proportion to the signal present in the composite image. Shown here is a Radon plane at radius r, polar angle θ, and azimuthal angle ϕ. P (r,θ,ϕ) is the projection value representing the sum of signals in the plane.

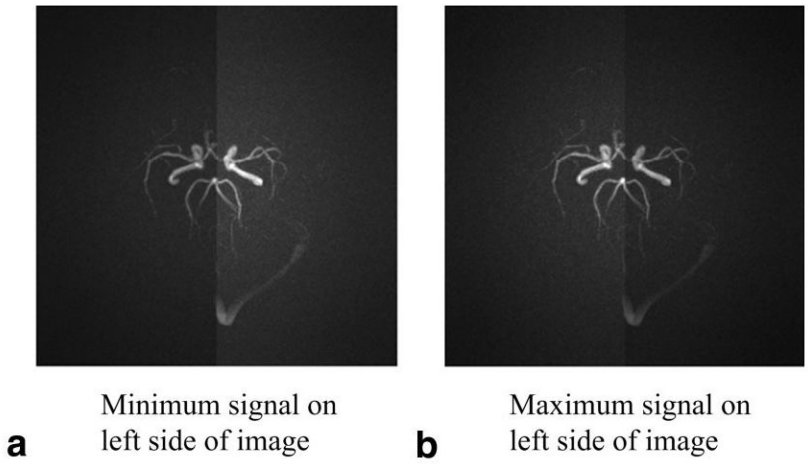

FIG. 3.
Images from the modulated time series used for Simulation 1. The right side of the image is constant in time. The left side is sinusoidally modulated in time.

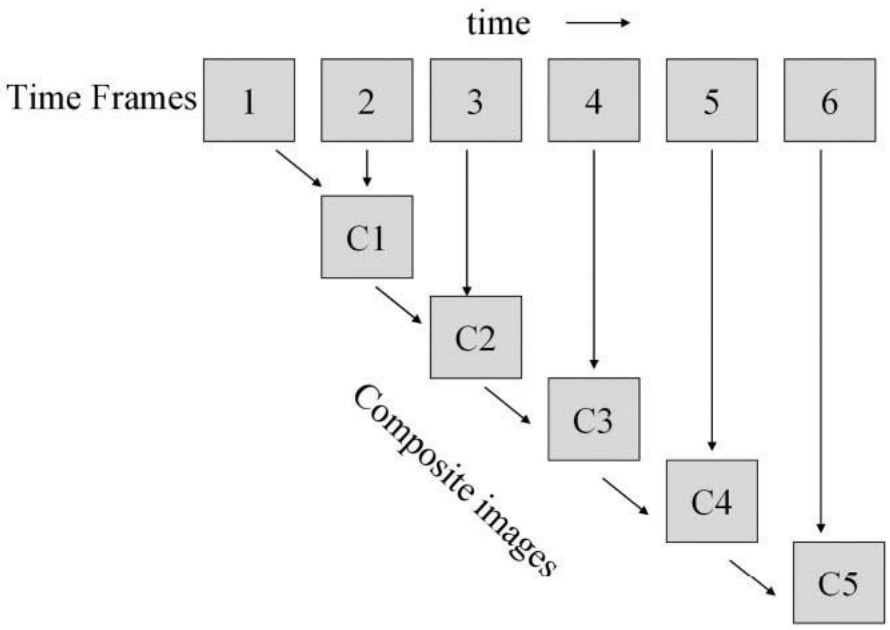

FIG. 4.

Illustration of the formation of progressive composite images for use in contrast enhanced time-resolved angiography. The first composite is formed from 2 or more time frames. As additional time frames are acquired, their information is added to the composite image.

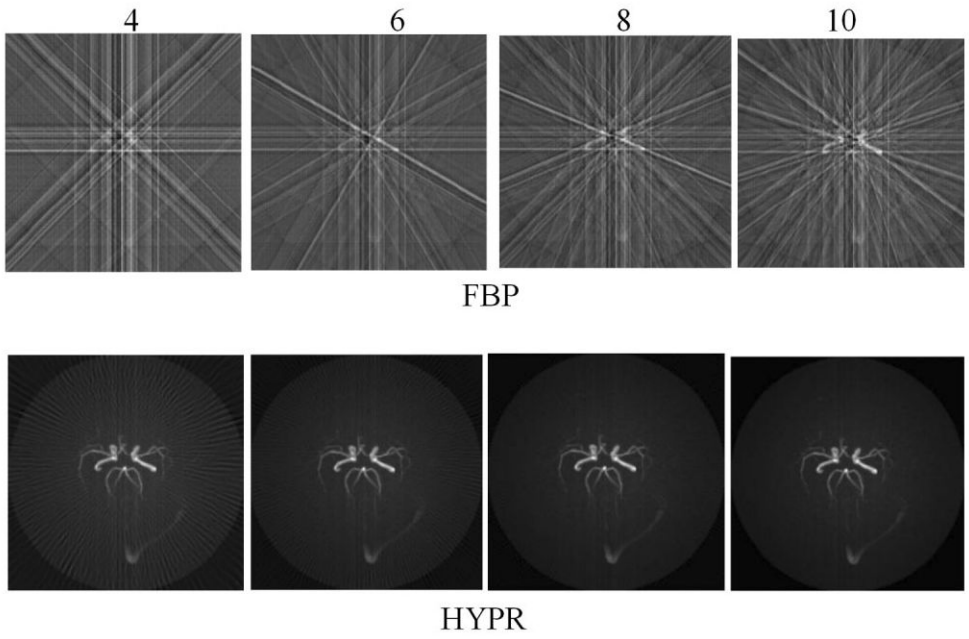

FIG. 5.
Comparison of under-sampled standard filtered back-projection (FBP) and HYPR images formed from 4, 6, 8, and 10 projections. A time series containing 16 frames was used in this example.

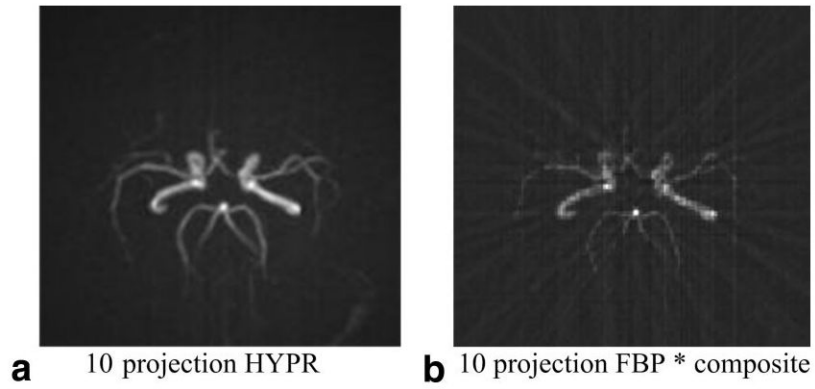

FIG. 6.

Comparison of 10-projection HYPR image (a) with an image formed as a product of a 10-projection FBP multiplied by the composite image (b). The image in (b) retains the basic FBP intravascular streak artifacts.

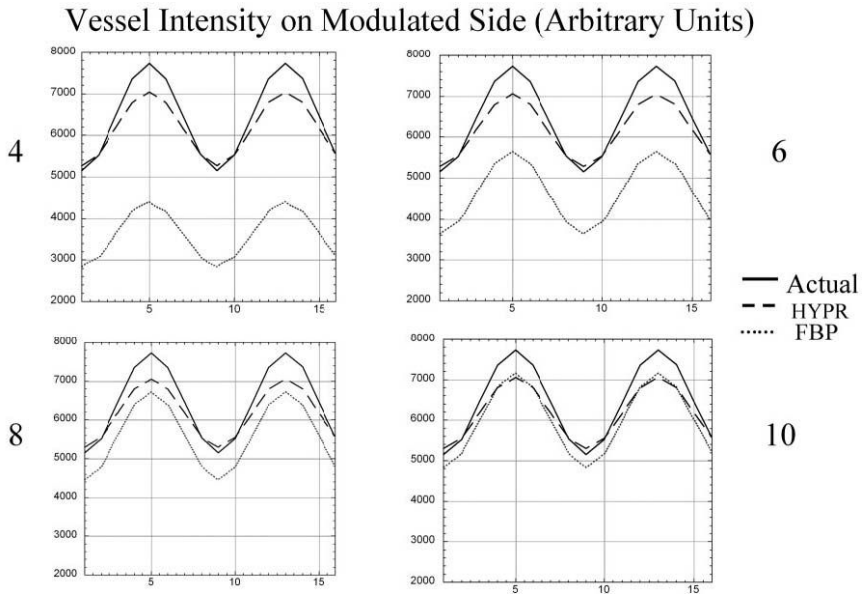

FIG. 7.

Comparison of programmed (Actual) waveform with those obtained from FBP and HYPR images with 4, 6, 8, and 10 projections for the modulated side of the image. The FBP waveforms are initially underestimated but are close to the HYPR waveforms for 10 projections and above.

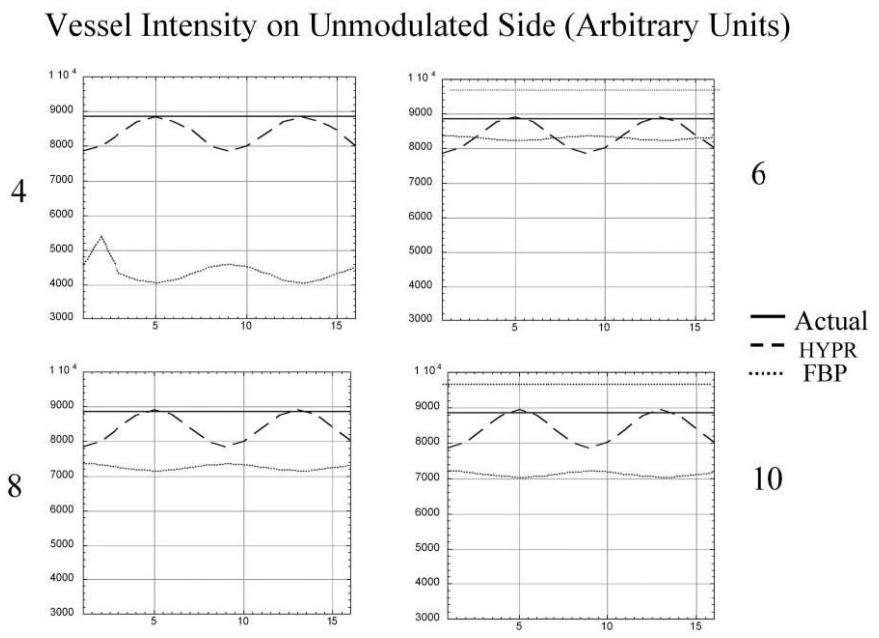

FIG. 8.

Comparison of programmed (Actual) waveform with those obtained from FBP and HYPR images with 4, 6, 8, and 10 projections for the unmodulated side of the image. Once again the FBP values underestimate the Actual constant waveform. The HYPR waveform shows some contamination from the left side in this example of spatial variation of the temporal waveform.

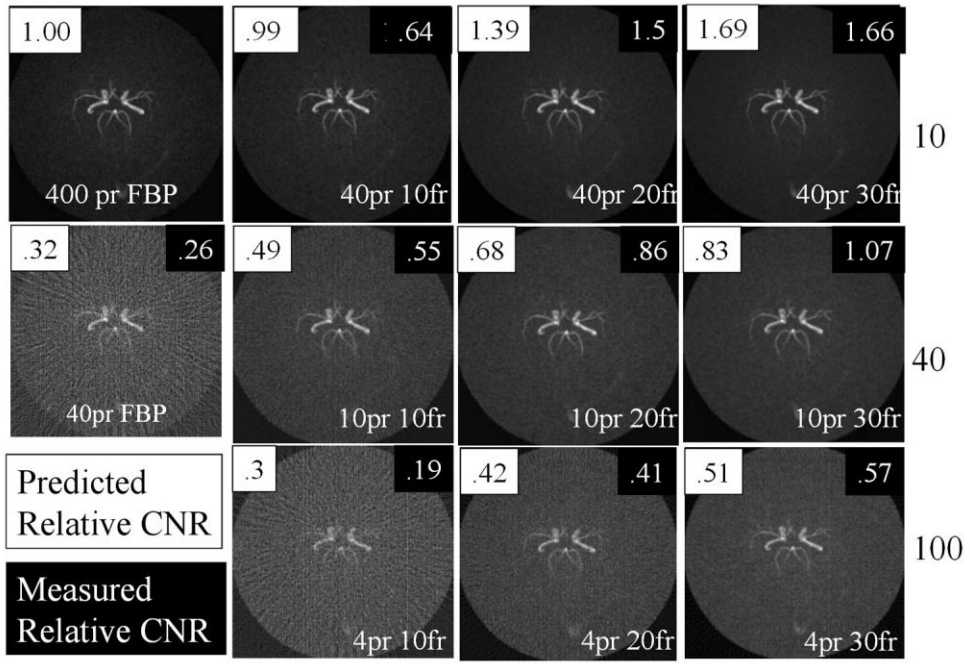

FIG. 9.

Comparison of image quality of an undersampled FBP image obtained with 40 projections with that of HYPR images obtained with various numbers of projections (pr) and numbers of frames (fr) in the time series. For a 30-frame acquisition, the HYPR technique provides a factor of 100 undersampling factor. Image quality is better than the FBP technique, which provides a factor of 10 undersampling factor relative to a fully sampled (400 projection) image. For the same number of projections, the FBP and HYPR images require equal acquisition times. Total scan time is proportional to the product of the number of projections and number of frames. Undersampling factors are shown on the right.

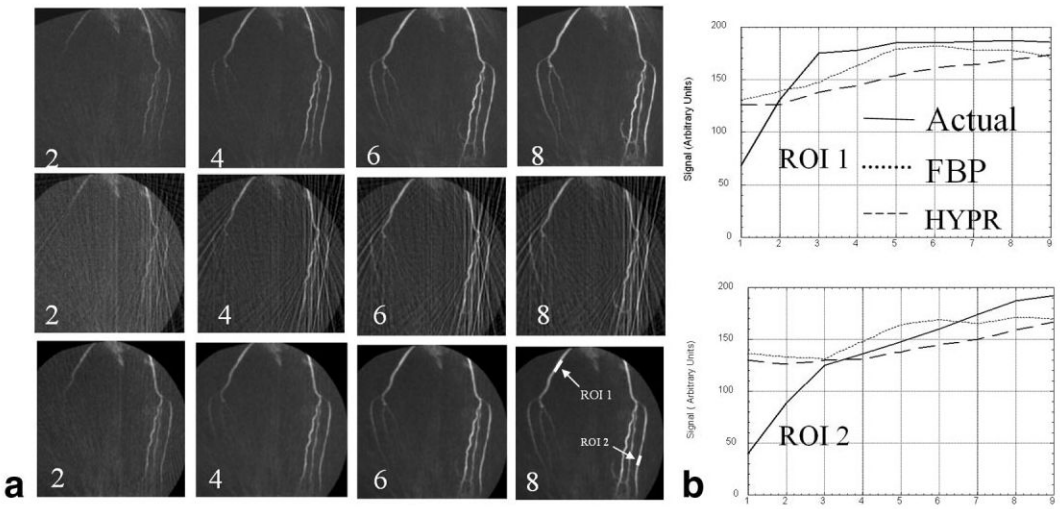

FIG. 10.

(**a**) Simulation 3. Top row: frames 2, 4, 6, and 8 from a clinical PR TRICKS examination that used 150 projections per time frame. Middle row: 30 projection FBP with undersampling factor of 13. Severe streaks are evident. Bottom row: 30 projection HYPR images. Image quality improves later in the exam because of increased projections in the composite image. (**b**) Signal curves for Simulation 3. FBP and HYPR signals are higher than Actual for the first 2 frames due to background signal. HYPR estimate improves as frames are added to the composite image.

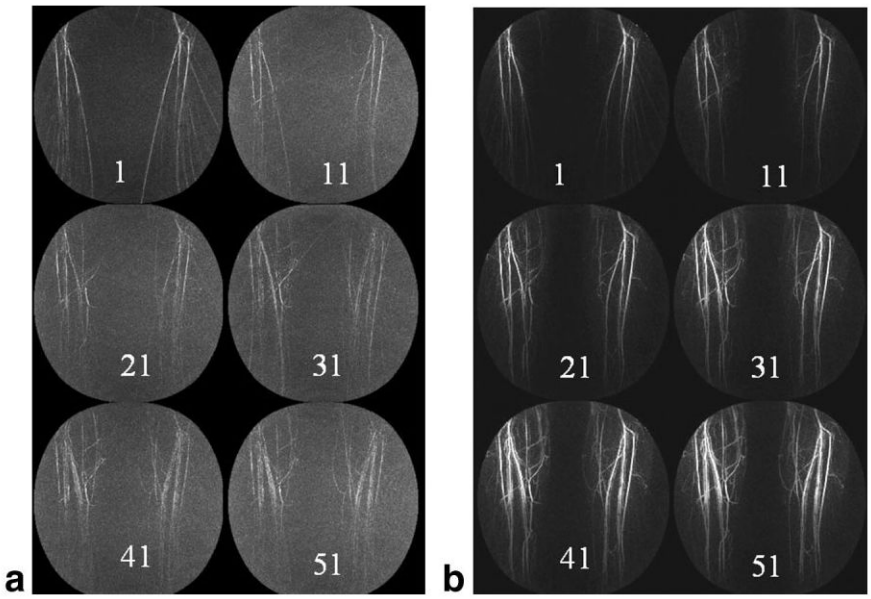

FIG. 11.

Every tenth frame of a PR TRICKS time series using 10 projections per 940ms time frame. The combined k-t undersampling factor = 225. Conventional PR TRICKS is shown in (**a**). HYPR PR TRICKS is shown in (**b**).

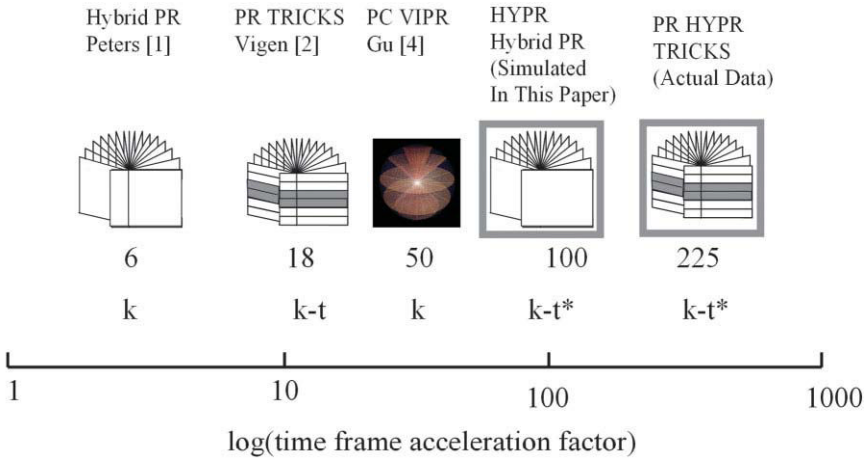

FIG. 12.

Time frame acceleration factors for several acquisition techniques. The acceleration factors indicate the time savings for individual time frames relative to fully sampled radial acquisition. Scan time is the product of this time and the number of frames. HYPR acceleration factor estimates presume a time series of 10–30 time frames. Acceleration factors do not includethe potential benefits of combination with parallel imaging techniques. HYPR acquisition parameters have been chosen to maintain current image quality in spite of higher accelerations.